arXiv:2107.03419v2 [hep-ex] 8 Dec 2021

Observation of excited Ω_c^0 baryons in $\Omega_b^- \to \Xi_c^+ K^- \pi^-$ decays

LHCb collaboration[†]

Abstract

The first observation of the $\Omega_b^- \to \Xi_c^+ K^- \pi^-$ decay is reported using pp collision data at centre-of-mass energies of 7, 8 and 13 TeV collected by the LHCb experiment, corresponding to an integrated luminosity of 9 fb^{-1}. Four excited Ω_c^0 baryons are observed in the $\Xi_c^+ K^-$ mass projection of the $\Omega_b^- \to \Xi_c^+ K^- \pi^-$ decays with the significance of each exceeding five standard deviations. They coincide with the states previously observed in prompt pp and $e^+ e^-$ production. Relative production rates, masses and natural widths of the states are measured, and a test of spin hypotheses is performed. Moreover, the branching ratio of $\Omega_b^- \to \Xi_c^+ K^- \pi^-$ is measured relative to the $\Omega_b^- \to \Omega_c^0 \pi^-$ decay mode and a precise measurement of the Ω_b^- mass of $6044.3 \pm 1.2 \pm 1.1 \, {}^{+0.19}_{-0.22}$ MeV is obtained.

[†]Authors are listed at the end of this Letter.

1 Introduction

The spectrum of the baryons with a single heavy quark Qqq' ($Q = b$ or c and $q, q' = u, d$ or s) is well classified using the heavy quark-diquark degrees of freedom. Heavy quark effective theory [1–8] provides the basis for factoring out the heavy-quark dynamics up to corrections of the first order of $1/m_Q$, where m_Q is the heavy quark mass. Therefore, the observation of new baryons and measurements of their properties provide information about the role played by diquarks in baryons, and can also help to tune tetraquark and pentaquark models.

In recent years, the LHCb experiment has made numerous contributions to the spectroscopy of heavy baryons by observing several new states [9–16]. Among them, the spectrum of excited Ω_c^0 baryons has drawn special attention. Five new excited narrow Ω_c^0 states, herein denoted Ω_c^{**0}, and promptly produced in proton-proton (pp) collisions, have been observed in the $\Xi_c^+ K^-$ mass spectrum [16, 17].

Many theoretical approaches including potential models, QCD sum rules, and lattice QCD predict the Ω_c^{**0} spectrum and interpret the newly discovered states as orbitally or radially excited Ω_c^0 states [18–36], while a few studies suggest that some of them may be either molecular states or pentaquarks [37–43]. Most of the predictions propose the mass ordering of the states, while widths and relative production rates remain unexploited on the theoretical side. Seven excited P-wave Ω_c^0 baryons are expected: five λ-mode excited states where the constituent c quark and the ss diquark are in a P-wave, and two ρ-mode excited states where the two s quarks are in a P-wave. One of the most popular interpretations is that the observed Ω_c^{**0} states correspond to the five λ-mode excited Ω_c^0 baryons with quantum numbers $J^P = 1/2^-, 1/2^-, 3/2^-, 3/2^-$, and $5/2^-$. The determination of the spin-parity quantum numbers of the Ω_c^{**0} states would help to discriminate between the proposed models and to probe the internal structure of the baryons.

This letter presents the first observation of the Ω_c^{**0} states produced in exclusive Ω_b^- decays. These are studied in the previously unobserved $\Omega_b^- \to \Xi_c^+ K^- \pi^-$ decays [44, 45], where the Ξ_c^+ baryons are reconstructed in the $pK^- \pi^+$ final state. The mass of the Ω_b^- baryon has been measured in decays to the $\Omega_c^0 \pi^-$ and $\Omega^- J/\psi$ final states. The new decay mode $\Omega_b^- \to \Xi_c^+ K^- \pi^-$ is a prominent reaction to measure also the Ω_b^- mass due to a multi-particle final state and smaller phase space with respect to the $\Omega_c^0 \pi^-$ mode.[1] The analysis is based on samples of pp collision data at centre-of-mass energies of $\sqrt{s} = 7, 8$ and $13 \, \text{TeV}$, corresponding to an integrated luminosity of $9 \, \text{fb}^{-1}$.

2 Detector and simulation

The LHCb detector [46, 47] is a single-arm forward spectrometer covering the pseudorapidity range $2 < \eta < 5$, designed for the study of particles containing b or c quarks. The detector includes a high-precision tracking system consisting of a silicon-strip vertex detector surrounding the pp interaction region, a large-area silicon-strip detector located upstream of a dipole magnet with a bending power of about $4 \, \text{Tm}$, and three stations of silicon-strip detectors together with straw drift tubes placed down-

---

[1]Unless otherwise stated, charge-conjugate processes are implicitly included, and natural units with $\hbar = c = 1$ are used throughout.

stream of the magnet. Simulation is necessary to train a multivariate algorithm used to suppress background, model shapes of mass distributions, and calculate efficiencies. In the simulation, pp collisions are generated using PYTHIA [48] with a specific LHCb configuration [49]. Decays of unstable particles are described by EVTGEN [50]. The interaction of the generated particles with the detector is implemented using the GEANT4 toolkit [51] as described in Ref [52].

3   Selection of $\Omega_b^- \to \Xi_c^+ K^- \pi^-$ decays

The Ξ_c^+ candidates are formed by combining three tracks that are detached from any primary pp interaction vertex (PV) in the event. A good-quality vertex fit is required to select tracks originating from the same secondary vertex. The Ω_b^- candidates are selected by combining the Ξ_c^+ candidate with two tracks identified as a K^- and a π^- meson. Loose particle identification (PID) requirements are applied to all five final-state tracks in order to reduce background. The Ω_b^- candidates are required to have a transverse momentum $p_T > 3.5\,\text{GeV}$ and are constrained to originate from the PV by requiring a small χ_{IP}^2, where χ_{IP}^2 is defined as the difference in the vertex-fit χ^2 of a given PV reconstructed with and without the candidate under consideration. The Ω_b^- decay time is required to be larger than $0.2\,\text{ps}$, making the overlap with the prompt sample analysed in Ref. [16] negligible.

A boosted decision tree (BDT) classifier, implemented using the TMVA toolkit [53], is used to further reduce the background. Variables found to provide good discrimination between signal and background are: the PID information and p_T of the final-state tracks, the Ξ_c^+ p_T, the Ξ_c^+ and Ω_b^- χ_{IP}^2, the Ξ_c^+ and Ω_b^- vertex-fit χ^2, the Ω_b^- flight-distance significance, defined as the measured flight distance divided by its uncertainty, and the cosine of the Ξ_c^+ and Ω_b^- direction angles. The direction angle is defined as the angle between the Ξ_c^+ (Ω_b^-) momentum and the vector joining the PV and the Ξ_c^+ (Ω_b^-) decay vertex. The training of the BDT classifier is performed using simulated samples as signal and data as background separately for Run 1 and Run 2 data samples. The candidates used for the background sample are in the 6200–6300 MeV range of the $\Xi_c^+ K^- \pi^-$ mass spectrum, which is not populated by partially reconstructed Ω_b^- decays. The optimal selection criterion on the BDT response is found by maximising the figure of merit $\epsilon/(5/2 + \sqrt{B_P})$ [54], where ϵ is the signal efficiency in simulation, and B_P is the number of $\Xi_c^+ K^- \pi^-$ candidates in the mass region $6200 < m(\Xi_c^+ K^- \pi^-) < 6256\,\text{MeV}$, roughly matching the expected number of background events in the Ω_b^- mass window. Roughly 4% of selected events contain more than one candidate and are removed. Finally, a kinematic fit [55] is applied to the Ω_b^- decays to improve the mass resolution where the Ξ_c^+ candidate mass is constrained to its known value [56], and the Ω_b^- candidate is constrained to originate from its associated PV, defined as the PV to which the impact parameter of the combination of two-track and Ξ_c^+ candidate is the smallest.

The resulting $\Xi_c^+ K^- \pi^-$ mass spectrum is shown in Fig. 1 (left) and an extended unbinned maximum-likelihood fit is performed. The signal shape is modelled by the combination of two Gaussian functions with a common mean, where the ratios of the resolutions and yields between the functions are fixed according to the simulation. The main sources of background are due to the partially reconstructed decays $\Omega_b^- \to \Xi_c^+ K^- \rho^-(\to \pi^- \pi^0)$ and $\Omega_b^- \to \Xi_c'^+(\to \Xi_c^+ \gamma)K^- \pi^-$, where the π^0 and γ are not reconstructed. The combinatorial
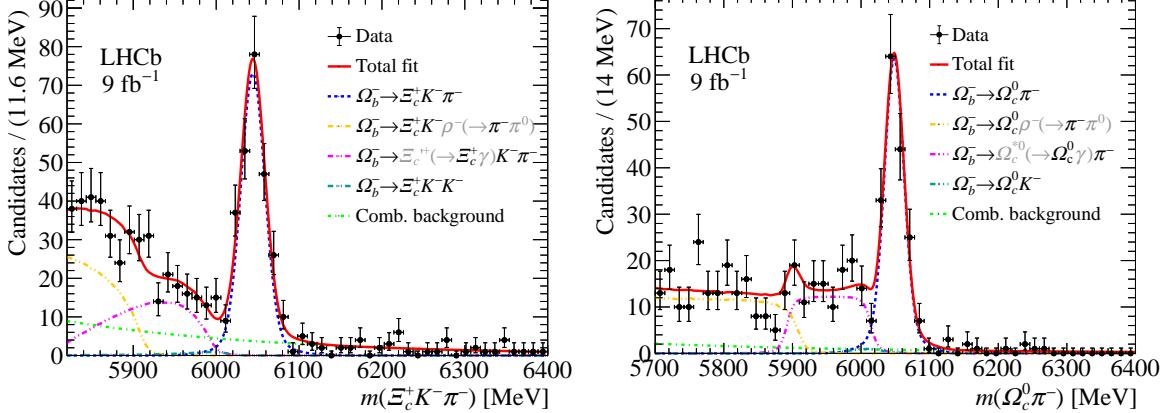
Figure 1: Distribution of the reconstructed invariant mass (left) $m(\Xi_c^+ K^- \pi^-)$ with $\Xi_c^+ \to p K^- \pi^+$ and (right) $m(\Omega_c^0 \pi^-)$ with $\Omega_c^0 \to p K^- K^- \pi^+$ for all candidates passing the selection requirements. The black symbols show the data. The result of a fit is overlaid (solid red line). The missing particles in partially reconstructed decays are indicated in grey in the legends.

background shape is fixed according to a wrong-sign sample, consisting of $\Xi_c^+ K^- \pi^+$ combinations processed in the same way as the right-sign $\Xi_c^+ K^- \pi^-$ combinations. The shape of the partially reconstructed decays is taken from simulated samples generated using the RapidSim package [57]. The shape of misidentified decays $\Omega_b^- \to \Xi_c^+ K^- K^-$ is fixed based on simulation. The yield ratio $N_{\Xi_c^+ K^- K^-}/N_{\Xi_c^+ K^- \pi^-}$ is fixed to 2.8% based on $|V_{us}|^2/|V_{ud}|^2 \approx 5\%$ corrected by the difference in reconstruction efficiency and the phase space. The fit returns a combined mass resolution of $17.9 \pm 1.3\,\mathrm{MeV}$, a yield of $N_{\Xi_c^+ K^- \pi^-} = 240 \pm 17$ and an Ω_b^- mass, $m(\Omega_b^-) = 6044.3 \pm 1.2$ MeV, where the uncertainty is statistical only (see Table 1). The Dalitz plot distribution of the candidates, with a mass within two standard deviations of the Ω_b^- peak, is shown in Fig. 2. Excited Ω_c^0 baryons appear in the $\Xi_c^+ K^-$ projection while no excited Ξ_c^0 states are clearly visible in the $\Xi_c^+ \pi^-$ system.

The branching fraction of $\Omega_b^- \to \Xi_c^+ K^- \pi^-$ decays is measured relative to the normalisation channel $\Omega_b^- \to \Omega_c^0 \pi^-$, with $\Omega_c^0 \to p K^- K^- \pi^+$. Similar selection requirements as the $\Omega_b^- \to \Xi_c^+ K^- \pi^-$ mode are applied to the $\Omega_b^- \to \Omega_c^0 \pi^-$ candidates. The selections of the two decay modes differ in the requirements applied to the invariant mass of the $p K^- \pi^+$ and $p K^- K^- \pi^+$ systems to select Ξ_c^+ and Ω_c^0 candidates, respectively. A kinematic fit is applied to the Ω_b^- decay where the Ω_c^0 candidate mass is constrained to its known value [56]. The two largest background components are due to the partially reconstructed decays $\Omega_b^- \to \Omega_c^0 \rho^-(\to \pi^- \pi^0)$, and $\Omega_b^- \to \Omega_c^{*0}(\to \Omega_c^0 \gamma)\pi^-$. The result of an unbinned maximum-likelihood fit is overlaid to the data in Fig. 1 (right). All decays are modelled in the same way as for the $\Omega_b^- \to \Xi_c^+ K^- \pi^-$ channel. The combinatorial background shape is fixed according to the projection of the Ω_c^0 sidebands in the $\Omega_c^0 \pi^-$ mass spectrum, where the Ω_c^0 sidebands are defined as the 2650–2670 and 2720–2740 MeV ranges in the $p K^- K^- \pi^+$ invariant mass distribution. The yield of reconstructed Ω_b^- candidates is $N_{\Omega_c^0 \pi^-} = 174 \pm 14$, and the mass resolution is $18.4 \pm 1.5\,\mathrm{MeV}$.

The ratio of branching fractions is obtained as

$$\mathcal{R} \equiv \frac{\mathcal{B}(\Omega_b^- \to \Xi_c^+ K^- \pi^-)\,\mathcal{B}(\Xi_c^+ \to p K^- \pi^+)}{\mathcal{B}(\Omega_b^- \to \Omega_c^0 \pi^-)\,\mathcal{B}(\Omega_c^0 \to p K^- K^- \pi^+)} = 1.35 \pm 0.11 \;,$$

3
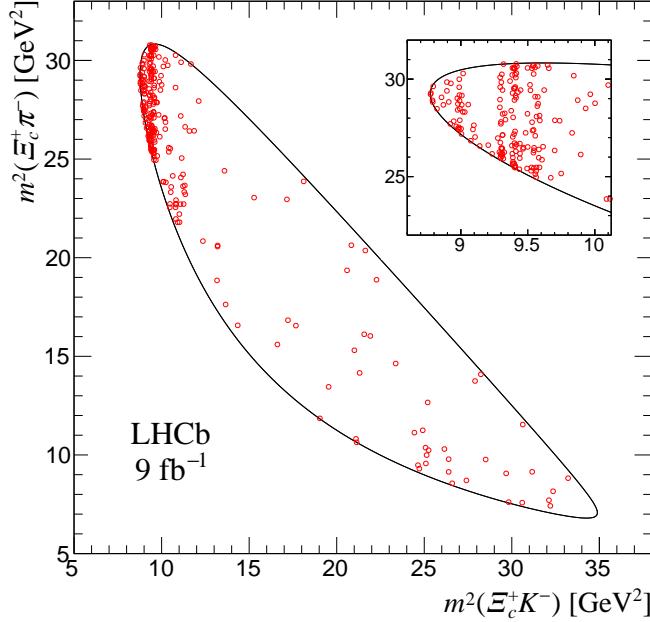
Figure 2: Dalitz plot distribution of $\Omega_b^- \to \Xi_c^+ K^- \pi^-$ candidates in the signal region, including background contributions. The inset shows an expanded view of the upper left corner where the vertical bands correspond to excited Ω_c^0 states.

which is calculated from the ratio of efficiency-corrected yields, where the error is statistical only (see Table 1).

4 The $\Xi_c^+ K^-$ mass spectrum

A search for excited Ω_c^0 baryons is performed in the $\Xi_c^+ K^-$ mass projection of $\Omega_b^- \to \Xi_c^+ K^- \pi^-$ candidates. In order to increase the selection efficiency of the Ω_c^{**0} states, an additional BDT classifier is deployed for the study of the $\Xi_c^+ K^-$ spectrum, where a sample of simulated $\Omega_b^- \to \Xi_c^+ K^- \pi^-$ decays, with an additional requirement of $m(\Xi_c^+ K^-) < 3.3\,\text{GeV}$, is used as the signal sample. For the background, the upper region of the $\Xi_c^+ K^- \pi^-$ mass distribution is used, as in the previous BDT classifier. After the optimization of the BDT response, the Ω_b^- candidates with a mass within two standard deviations of the Ω_b^- peak are selected. Figure 3 shows the distribution of the mass difference $\Delta M \equiv m(\Xi_c^+ K^-) - m_{\Xi_c^+} - m_{K^-}$, where $m(\Xi_c^+ K^-)$ is the invariant mass of the $\Xi_c^+ K^-$ system, and $m_{\Xi_c^+}$ and m_{K^-} are the world averages of the Ξ_c^+ and K^- masses, respectively [56]. Four narrow peaking structures are clearly visible close to the $\Xi_c^+ K^-$ kinematic threshold.

An extended maximum-likelihood fit is performed to the ΔM distribution, where each signal is modelled by an S-wave relativistic Breit-Wigner (BW) function multiplied by the phase space function and convolved with a Gaussian function to describe the mass resolution. The widths and masses of the relativistic BW functions vary freely. The background consists of two components: the combinatorial background under the Ω_b^- signal peak (Fig. 1 (left)) and the nonresonant $\Xi_c^+ K^-$ component. The former (combinatorial)

4
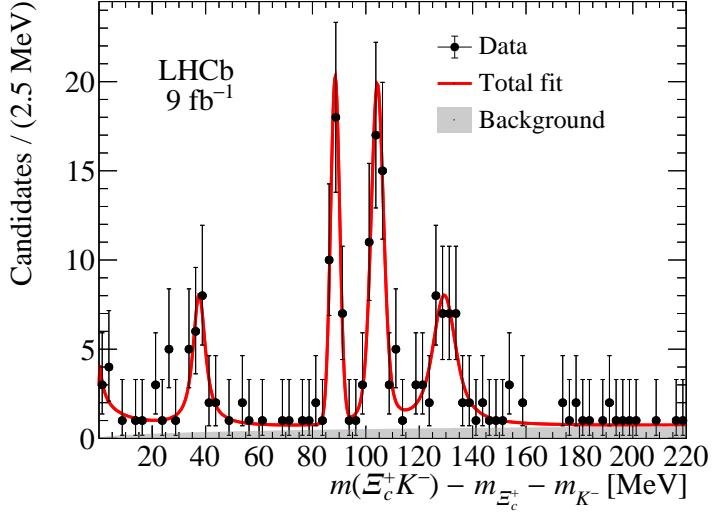
Figure 3: Distribution of the reconstructed mass difference between the $\Xi_c^+ K^-$ invariant mass and the Ξ_c^+ and K^- masses. The four peaking structures are consistent with being the previously observed $\Omega_c(3000)^0$, $\Omega_c(3050)^0$, $\Omega_c(3065)^0$ and $\Omega_c(3090)^0$ baryons. The distribution shows an enhancement at the threshold, as seen in the previous analysis [16]. The total fit is overlaid in red. The background distribution (grey shaded area) is the combination of the combinatorial and nonresonant $\Xi_c^+ K^-$ backgrounds.

is modelled by projecting the Ω_b^- sideband into the $\Xi_c^+ K^-$ invariant mass distribution and the latter (nonresonant $\Xi_c^+ K^-$) according to phase space. While the shapes of the two contributions and the yield of the combinatorial component are fixed, the yield of the nonresonant background can vary freely. The $\Xi_c^+ K^-$ spectrum also features an excess at the $\Xi_c^+ K^-$ mass threshold which is modelled by an S-wave BW component. Fit results superimposed to the data are shown in Fig. 3. The yields attributed to the four peaks are 24 ± 7, 33 ± 6, 51 ± 8, and 41 ± 9 respectively. The resulting BW parameters of the four signals, which are listed in Table 1, are consistent with those of the previously observed $\Omega_c(3000)^0$, $\Omega_c(3050)^0$, $\Omega_c(3065)^0$ and $\Omega_c(3090)^0$ baryons [16]. The natural width of the $\Omega_c(3050)^0$ is consistent with zero, therefore an upper limit is set. In order to determine the significance of the peaking structures, another fit is performed by fixing the masses and widths of the Ω_c^{**0} states to the previously measured values [16]. Therefore, the statistical significance of each peak is calculated using $\sqrt{2\Delta(\mathrm{NLL})}$, where $\Delta(\mathrm{NLL})$ is the variation of the fit log-likelihood when the corresponding BW function is excluded from the reference fit model. The local significance exceeds six standard deviations $(6\,\sigma)$ for each of the four main states. For the threshold structure, the null hypothesis of the background fluctuation is tested using the likelihood ratio of two fits. The p-value expressed in standard deviations using the one-sided convention corresponds to $4.3\,\sigma$ after systematic uncertainties are accounted for. Finally, the production rate of the Ω_c^{**0} states relative to the $\Omega_b^- \to \Xi_c^+ K^- \pi^-$ mode is defined as

$$\mathcal{P}_{\Omega_c^{**0}} \equiv \frac{\mathcal{B}(\Omega_b^- \to \Omega_c^{**0} \pi^-)\,\mathcal{B}(\Omega_c^{**0} \to \Xi_c^+ K^-)}{\mathcal{B}(\Omega_b^- \to \Xi_c^+ K^- \pi^-)}\,. \tag{1}$$

The rate is measured for the $\Omega_c(3000)^0$, $\Omega_c(3050)^0$, $\Omega_c(3065)^0$ and $\Omega_c(3090)^0$, and an upper limit on the production of the $\Omega_c(3120)^0$ state is set. The results are reported in

Table 1 with the statistical error computed using the binomial distribution.

5 Spin test for the excited Ω_c^0 baryons

In order to probe the spin of the Ω_c^{**0} baryons, the distribution of the helicity angle in the $\Omega_b^- \to \Omega_c^{**0}(\to \Xi_c^+ K^-)\pi^-$ decay is studied. The helicity angle θ is defined as the angle between the $\vec{p}_{K^-}$ and the $-\vec{p}_{\pi^-}$ directions in the $\Xi_c^+ K^-$ rest frame, where $\vec{p}$ is the momentum of the meson. The spin projection of the Ω_c^{**0} baryon in the direction of the π^- meson is limited to $1/2$ as it is produced in the $\Omega_b^- \to \Omega_c^{**0}\pi^-$ decay. Additionally, it cannot exceed $1/2$ in the direction of either decay product, Ξ_c^+ or K^-, due to their spins. Therefore, the angular distribution for a Ω_c^{**0} state with spin J is given as

$$I_J(\cos\theta) = \frac{(2J+1)}{2}\left(\left|d^J_{1/2,-1/2}(\cos\theta)\right|^2 + \left|d^J_{1/2,+1/2}(\cos\theta)\right|^2\right), \qquad (2)$$

where $d^J_{\nu,\lambda}$ is the Wigner d-function. The first (second) index, ν (λ), gives the spin projections of the Ω_c^{**0} in the direction opposite to the pion (kaon) momentum, $-\vec{p}_{\pi^-}$ ($-\vec{p}_{K^-}$), in the $\Xi_c^+ K^-$ rest frame. The angular distributions are not affected by a possible polarization of the Ω_b^- baryon since its production angles are integrated over. The Ω_c^{**0} candidates are selected in the small nonoverlapping regions around the peaks. The $\cos\theta$ distributions for the Ω_c^{**0} states are shown in Fig. 4. The $\Omega_c(3050)^0$ and $\Omega_c(3065)^0$ distributions show an enhancement at $\cos\theta = -1$, hinting at a preference for a spin larger than $J = 1/2$.

The expectations for the angular density function, $D_J(\cos\theta)$, shown by the colored lines in Fig. 4, are calculated as a sum of the signal PDF and the two background components (combinatorial and nonresonant $\Xi_c^+ K^-$) by

$$D_J(\cos\theta) \equiv f_s I_J(\cos\theta)\epsilon(\cos\theta) + f_b B_1(\cos\theta) + (1 - f_s - f_b)B_2(\cos\theta)\epsilon(\cos\theta), \qquad (3)$$

where f_s and f_b are the fractions of the signal and the combinatorial background fixed according to the result of the mass fit. The angular distribution for the combinatorial background, $B_1(\cos\theta)$, is fixed by selecting candidates in the $\Xi_c^+ K^- \pi^-$ mass range above the Ω_b^- peak. A flat distribution is assumed for nonresonant background, $B_2(\cos\theta)$. The efficiency, $\epsilon(\cos\theta)$, is calculated separately for each signal region using simulation. The efficiency maps are combined according to the fraction of the signal candidates in the corresponding data-taking periods. The efficiency for the helicity angle is calculated by convolving the efficiency map with the Ω_c^{**0} line-shape profile. The fall of the curves at $\cos\theta = 1$ indicates the smaller reconstruction efficiency for candidates with a low momentum K^- in the Ω_b^- rest frame. Discrimination of different spin hypotheses is based on the likelihood-ratio test statistic,

$$t_{H_J|H_{J'}} = \frac{1}{N}\sum_{i=1}^{N}\log\left[D_{H_J}(\cos\theta_i)/D_{H_{J'}}(\cos\theta_i)\right], \qquad (4)$$

where H_J and $H_{J'}$ are the compared hypotheses for the state to have spin J and J', respectively, N is the number of candidates in the mass region around the peak. The test statistic $\vec{t}^{\,(\text{data})} = (t^{(\text{data})}_{J=1/2|J=3/2}, t^{(\text{data})}_{J=3/2|J=5/2})$ is evaluated in data and compared to the t distribution in simulated pseudoexperiments. A set of $20\,000$ pseudoexperiments with
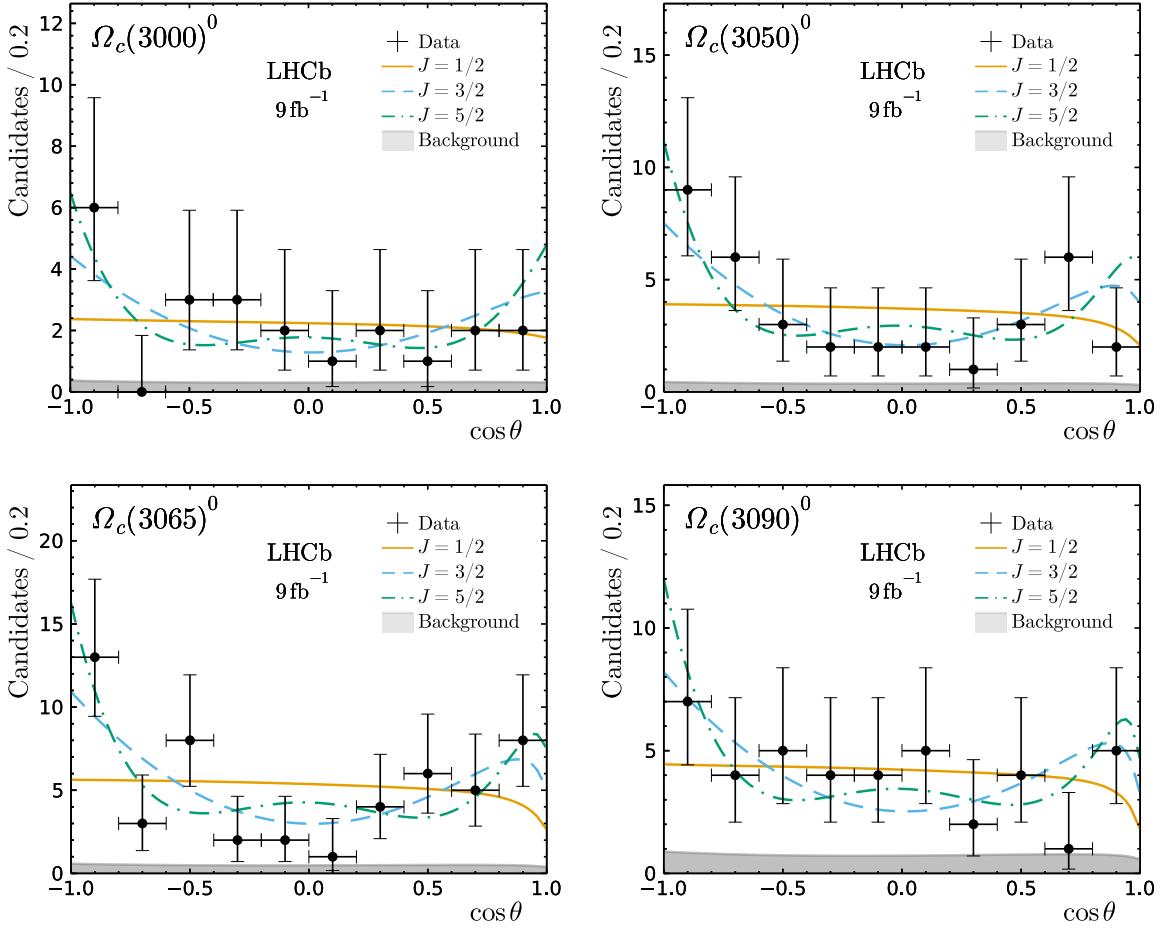
Figure 4: Distributions of the Ω_c^{**0} helicity angle (θ) in the Ω_b^- decay. Solid, dashed and dot-dashed lines indicate the expectations under the spin hypotheses, $J = 1/2$, $3/2$, and $5/2$, respectively. The grey shaded area shows the cumulative distribution of the combinatorial and nonresonant $\Xi_c^+ K^-$ backgrounds.

the number of signal and background events obtained from data are simulated for each spin hypothesis and for every Ω_c^{**0} state. The two-dimensional distribution of t is well described by the multivariate normal distribution from which we extract the covariance matrix and the two-dimensional mean, $t^{(\text{mean})}$. The p-value in the double-tailed convention is calculated by $\exp(-r^2/2)$, where r is the Mahalanobis distance [58] between $\vec{t}^{(\text{data})}$ and $\vec{t}^{(\text{mean})}$. All results are summarized in Table 1. The significance of the rejection of the $J = 1/2$ hypothesis for $\Omega_c(3050)^0$ and $\Omega_c(3065)^0$ is $2.2\,\sigma$ and $3.6\,\sigma$ respectively, including systematic effects listed in the next section. The combined hypothesis of the four peaks to have quantum numbers in the order $1/2$, $1/2$, $3/2$, $3/2$ is tested and rejected with a significance of $3.5\,\sigma$.

6   Systematic uncertainties

Various systematic uncertainties for each observable are considered, where the largest deviation from the default model on every source is used. A summary of the systematic

uncertainties is provided in the supplemental material [59]. The uncertainties from different sources are combined in quadrature. A source of systematic uncertainty is determined from varying components of the Ω_b^- fit model. The helicity couplings of the partially reconstructed decays in the $\Omega_c^0\pi^-$ invariant mass spectrum are modified as well as the shape used to describe the signal peaks. The uncertainty in the yield of misidentified decays is quantified by varying the fractional contribution by $\pm 40\%$ relative to the default value. In simulation, the $\Xi_c^+ \to pK^-\pi^+$ Dalitz plot is generated according to phase space and a binned weighting is performed to match the data. A systematic uncertainty is found by varying the binning scheme.

The uncertainty in the mass measurements due to momentum calibration is determined following Ref. [60] as $\pm 0.03\%$ of the energy released in the decay. The PID variables in simulation are corrected in order to match the PID performance in data. To calculate an uncertainty, a modified weighting is applied to the PID variables. For the uncertainty in the Ω_b^- kinematics, the p_{T} and η of the Ω_b^- candidates, as well as the track multiplicity in simulation, are weighted according to data. Several alternative models are considered for $\Xi_c^+K^-$ fit. Firstly, the resolution of each Gaussian function is varied by $\pm 10\%$. In addition, different orbital angular momenta ($L = 1, 2$) are tested along with the variation of the Blatt-Weisskopf factors [61,62] from 1.5 to $5\,\mathrm{GeV}^{-1}$. A constant-width BW approximation and the scattering-length approximation are probed for the threshold structure. Lastly, for each signal peak, interference with neighbours and the nonresonant $\Xi_c^+K^-$ background is tested. The full list of results including systematic uncertainties are listed in Table 1.

7 Summary and conclusion

In summary, data collected by the LHCb experiment at centre-of-mass energies 7, 8 and $13\,\mathrm{TeV}$ corresponding to an integrated luminosity of $9\,\mathrm{fb}^{-1}$ are used to observe the new decay mode $\Omega_b^- \to \Xi_c^+K^-\pi^-$ and to measure its branching fraction relative to the $\Omega_b^- \to \Omega_c^0\pi^-$ decay mode. A precise measurement of the Ω_b^- mass, $m(\Omega_b^-) = 6044.3\pm1.2\pm1.1\,^{+0.19}_{-0.22}\,\mathrm{MeV}$, is obtained where the first uncertainty is statistical, the second is systematic, and the third asymmetric error is due to the uncertainty in the Ξ_c^+ mass. Averaging with the previous LHCb measurements [63, 64], taking correlated systematic uncertainties into account, gives a mass of $m(\Omega_b^-) = 6044.8 \pm 1.3\,\mathrm{MeV}$, which is the most precise to date.

The investigation of the $\Xi_c^+K^-$ mass spectrum has revealed four excited Ω_c^0 baryons, $\Omega_c(3000)^0$, $\Omega_c(3050)^0$, $\Omega_c(3065)^0$, $\Omega_c(3090)^0$, and a threshold enhancement as also seen in Ref. [16]. The $\Omega_c(3120)^0$ state is not observed, therefore an upper limit on its production rate is set by scanning the likelihood profile, $\mathcal{P}_{\Omega_c(3120)^0} < 0.03$ at 95% confidence level (CL). Measurements of the Ω_c^{**0} masses and widths, together with an upper limit of $\Gamma_{\Omega_c(3050)^0} < 1.6\,\mathrm{MeV}$ at 95% CL are reported. Their spin assignments are tested based on the distribution of the helicity angle in the decay chain $\Omega_b^- \to \Omega_c^{**0}\pi^-$, $\Omega_c^{**0} \to \Xi_c^+K^-$. Significance values of excluding the $J = 1/2$ spin hypothesis for $\Omega_c(3050)^0$ and $\Omega_c(3065)^0$ are $2.2\,\sigma$ and $3.6\,\sigma$, respectively. All results are summarised in Table 1. The combined hypothesis on the spin of the four peaks in the order $J = 1/2, 1/2, 3/2, 3/2$, as proposed in several works [20, 31, 36], is rejected with a p-value corresponding to 3.5 standard deviations once systematic uncertainties are taken into account.

The results of the angular analysis together to the absence of the $\Omega_c(3120)^0$ state in the $\Xi_c^+K^-$ spectrum in Ω_b^- decays and in e^+e^- collisions at Belle [17], suggest that the

interpretation of the five peaks observed in Ref. [16] as λ-mode excited states might be invalid. In such a scenario, only the four peaks observed in this analysis would be λ-mode excitations (with quantum numbers $J = 1/2$, $3/2$, $3/2$, and $5/2$) and a spin $1/2$ λ-mode state would be still to be observed. The nonobservation of the $\Omega_c(3120)^0$ baryon would be consistent with the state being either one of the $2S$ doublet, decaying to $\Xi_c^+ K^-$ in P-wave [27,31], or a ρ-mode P-wave excitation with spin $3/2^-$ that requires D-wave between Ξ_c^+ and K^-. Finally, the $\Xi_c^+ K^-$ spectrum also features an excess at the $\Xi_c^+ K^-$ mass threshold. An analogous enhancement was observed in the inclusive $\Xi_c^+ K^-$ spectrum [16] and interpreted as the partially reconstructed decay $\Omega_c(3065)^0 \to \Xi_c'^+ (\to \Xi_c^+ \gamma) K^-$ with the photon escaping detection. However, such an explanation does not hold here, given that the partially reconstructed decay $\Omega_b^- \to \Xi_c'^+ K^- \pi^-$ does not populate the mass region selected for the exclusive $\Omega_b^- \to \Xi_c^+ K^- \pi^-$ decay. While the current data do not provide enough sensitivity to determine the parameters of the structure, such as the mass, natural width and spin, future data acquired with the upgraded LHCb detector will provide insights to establish its nature.

Table 1: Results on the Ω_b^- mass, relative branching fraction of the $\Xi_c^+ K^- \pi^-$ decay mode, measured mass differences (ΔM), masses (m), natural widths (Γ) and production fraction ($\mathcal{P}$) of Ω_c^{**0} baryons where the first uncertainty is statistical and the second systematic. The third asymmetric uncertainty on the Ω_b^- and Ω_c^{**0} masses is due to the uncertainty in the Ξ_c^+ mass. Upper limits are given for the width of the $\Omega_c(3050)^0$ state and the production rate of the $\Omega_c(3120)^0$ baryon, which are measured to be consistent with zero. The results of the spin analysis are also listed (J rejection).

State	Observable	Measurement
Ω_b^-	m	$6044.3 \pm 1.2 \pm 1.1\,^{+0.19}_{-0.22}$ MeV
	$\mathcal{R}$	$1.35 \pm 0.11 \pm 0.05$
Threshold structure	Significance	$4.3\,\sigma$
$\Omega_c(3000)^0$	Significance	$6.2\,\sigma$
	ΔM	$37.6 \pm 0.9 \pm 0.9$ MeV
	m	$2999.2 \pm 0.9 \pm 0.9\,^{+0.19}_{-0.22}$ MeV
	Γ	$4.8 \pm 2.1 \pm 2.5$ MeV
	$\mathcal{P}$	$0.11 \pm 0.02 \pm 0.04$
	J rejection	$0.5\,\sigma\,(J=1/2), 0.8\,\sigma\,(J=3/2), 0.4\,\sigma\,(J=5/2)$
$\Omega_c(3050)^0$	Significance	$9.9\,\sigma$
	ΔM	$88.5 \pm 0.3 \pm 0.2$ MeV
	m	$3050.1 \pm 0.3 \pm 0.2\,^{+0.19}_{-0.22}$ MeV
	Γ	< 1.6 MeV, 95% CL
	$\mathcal{P}$	$0.15 \pm 0.02 \pm 0.02$
	J rejection	$2.2\,\sigma\,(J=1/2), 0.1\,\sigma\,(J=3/2), 1.2\,\sigma\,(J=5/2)$
$\Omega_c(3065)^0$	Significance	$11.9\,\sigma$
	ΔM	$104.3 \pm 0.4 \pm 0.4$ MeV
	m	$3065.9 \pm 0.4 \pm 0.4\,^{+0.19}_{-0.22}$ MeV
	Γ	$1.7 \pm 1.0 \pm 0.5$ MeV
	$\mathcal{P}$	$0.23 \pm 0.02 \pm 0.02$
	J rejection	$3.6\,\sigma\,(J=1/2), 0.6\,\sigma\,(J=3/2), 1.2\,\sigma\,(J=5/2)$
$\Omega_c(3090)^0$	Significance	$7.8\,\sigma$
	ΔM	$129.4 \pm 1.1 \pm 1.0$ MeV
	m	$3091.0 \pm 1.1 \pm 1.0\,^{+0.19}_{-0.22}$ MeV
	Γ	$7.4 \pm 3.1 \pm 2.8$ MeV
	$\mathcal{P}$	$0.19 \pm 0.02 \pm 0.04$
	J rejection	$0.3\,\sigma\,(J=1/2), 0.8\,\sigma\,(J=3/2), 0.5\,\sigma\,(J=5/2)$
$\Omega_c(3120)^0$	$\mathcal{P}$	< 0.03, 95% CL

Acknowledgements

References

[1] N. Isgur and M. B. Wise, *Weak decays of heavy mesons in the static quark approximation*, Phys. Lett. **B232** (1989) 113.

[2] N. Isgur and M. B. Wise, *Weak transition form factors between heavy mesons*, Phys. Lett. **B237** (1990) 527.

[3] B. Grinstein, *The static quark effective theory*, Nucl. Phys. **B339** (1990) 253.

[4] H. Georgi, *An effective field theory for heavy quarks at low energies*, Phys. Lett. **B240** (1990) 447.

[5] E. Eichten and B. R. Hill, *An effective field theory for the calculation of matrix elements involving heavy quarks*, Phys. Lett. **B234** (1990) 511.

[6] A. F. Falk, H. Georgi, B. Grinstein, and M. B. Wise, *Heavy meson form factors from QCD*, Nucl. Phys. **B343** (1990) 1.

[7] A. G. Grozin, *Introduction to the heavy quark effective theory*, arXiv:hep-ph/9908366.

[8] T. Mannel, *Effective theory for heavy quarks*, Lect. Notes Phys. **479** (1997) 387, arXiv:hep-ph/9606299.

[9] LHCb collaboration, R. Aaij *et al.*, *Observation of new Ξ_c^0 baryons decaying to $\Lambda_c^+ K^-$*, Phys. Rev. Lett. **124** (2020) 222001, arXiv:2003.13649.

[10] LHCb collaboration, R. Aaij *et al.*, *Observation of a new Ξ_b^0 state*, Phys. Rev. **D103** (2021) 012004, arXiv:2010.14485.

[11] LHCb collaboration, R. Aaij *et al.*, *Observation of a new baryon state in the $\Lambda_b^0\pi^+\pi^-$ mass spectrum*, JHEP **06** (2020) 136, arXiv:2002.05112.

[12] LHCb collaboration, R. Aaij *et al.*, *First observation of excited Ω_b^- states*, Phys. Rev. Lett. **124** (2020) 082002, arXiv:2001.00851.

[13] LHCb collaboration, R. Aaij *et al.*, *Observation of new resonances in the $\Lambda_b^0\pi^+\pi^-$ system*, Phys. Rev. Lett. **123** (2019) 152001, arXiv:1907.13598.

[14] LHCb collaboration, R. Aaij *et al.*, *Observation of two resonances in the $\Lambda_b^0\pi^\pm$ systems and precise measurement of $\Sigma_b^\pm$ and $\Sigma_b^{*\pm}$ properties*, Phys. Rev. Lett. **122** (2019) 012001, arXiv:1809.07752.

[15] LHCb collaboration, R. Aaij *et al.*, *Observation of a new Ξ_b^- resonance*, Phys. Rev. Lett. **121** (2018) 072002, arXiv:1805.09418.

[16] LHCb collaboration, R. Aaij *et al.*, *Observation of five new narrow Ω_c^0 states decaying to $\Xi_c^+ K^-$*, Phys. Rev. Lett. **118** (2017) 182001, arXiv:1703.04639.

[17] Belle collaboration, J. Yelton *et al.*, *Observation of excited Ω_c charmed baryons in e^+e^- collisions*, Phys. Rev. **D97** (2018) 051102, arXiv:1711.07927.

[18] G. Chiladze and A. F. Falk, *Phenomenology of new baryons with charm and strangeness*, Phys. Rev. **D56** (1997) R6738, arXiv:hep-ph/9707507.

[19] W. Wang and R.-L. Zhu, *Interpretation of the newly observed Ω_c^0 resonances*, Phys. Rev. **D96** (2017) 014024, arXiv:1704.00179.

[20] M. Padmanath and N. Mathur, *Quantum numbers of recently discovered Ω_c^0 baryons from lattice QCD*, Phys. Rev. Lett. **119** (2017) 042001, arXiv:1704.00259.

[21] H.-Y. Cheng and C.-W. Chiang, *Quantum numbers of Ω_c states and other charmed baryons*, Phys. Rev. **D95** (2017) 094018, arXiv:1704.00396.

[22] S. Capstick and N. Isgur, *Baryons in a relativized quark model with chromodynamics*, Phys. Rev. **D34** (1986) 2809.

[23] H. Huang, J. Ping, and F. Wang, *Investigating the excited Ω_c^0 states through $\Xi_c\bar{K}$ and $\Xi_c'\bar{K}$ decay channels*, Phys. Rev. **D97** (2018) 034027, arXiv:1704.01421.

[24] Z. Zhao, D.-D. Ye, and A. Zhang, *Hadronic decay properties of newly observed Ω_c baryons*, Phys. Rev. **D95** (2017) 114024, arXiv:1704.02688.

[25] B. Chen and X. Liu, *New Ω_c^0 baryons discovered by LHCb as the members of $1P$ and $2S$ states*, Phys. Rev. **D96** (2017) 094015, arXiv:1704.02583.

[26] S.-Q. Luo, B. Chen, X. Liu, and T. Matsuki, *Predicting a new resonance as charmed-strange baryonic analog of $D_{s0}^*(2317)$*, Phys. Rev. **D103** (2021) 074027, arXiv:2102.00679.

[27] V. O. Galkin and R. N. Faustov, *Heavy baryon spectroscopy*, Phys. Part. Nucl. **51** (2020) 661.

[28] W. Roberts and M. Pervin, *Heavy baryons in a quark model*, Int. J. Mod. Phys. **A23** (2008) 2817, arXiv:0711.2492.

[29] Z. Shah, K. Thakkar, A. Kumar Rai, and P. C. Vinodkumar, *Excited state mass spectra of singly charmed baryons*, Eur. Phys. J. **A52** (2016) 313, arXiv:1602.06384.

[30] T. Yoshida *et al.*, *Spectrum of heavy baryons in the quark model*, Phys. Rev. **D92** (2015) 114029, arXiv:1510.01067.

[31] M. Karliner and J. L. Rosner, *Very narrow excited Ω_c baryons*, Phys. Rev. **D95** (2017) 114012, arXiv:1703.07774.

[32] K.-L. Wang, L.-Y. Xiao, X.-H. Zhong, and Q. Zhao, *Understanding the newly observed Ω_c states through their decays*, Phys. Rev. **D95** (2017) 116010, arXiv:1703.09130.

[33] S. S. Agaev, K. Azizi, and H. Sundu, *Interpretation of the new Ω_c^0 states via their mass and width*, Eur. Phys. J. **C77** (2017) 395, arXiv:1704.04928.

[34] H.-X. Chen *et al.*, *Decay properties of P-wave charmed baryons from light-cone QCD sum rules*, Phys. Rev. **D95** (2017) 094008, arXiv:1703.07703.

[35] H.-X. Chen *et al.*, *P-wave charmed baryons from QCD sum rules*, Phys. Rev. **D91** (2015) 054034, arXiv:1502.01103.

[36] Z.-G. Wang, *Analysis of $\Omega_c(3000)$, $\Omega_c(3050)$, $\Omega_c(3066)$, $\Omega_c(3090)$ and $\Omega_c(3119)$ with QCD sum rules*, Eur. Phys. J. **C77** (2017) 325, arXiv:1704.01854.

[37] R. Chen, A. Hosaka, and X. Liu, *Searching for possible Ω_c-like molecular states from meson-baryon interaction*, Phys. Rev. **D97** (2018) 036016, arXiv:1711.07650.

[38] H.-C. Kim, M. V. Polyakov, and M. Praszałowicz, *Possibility of the existence of charmed exotica*, Phys. Rev. **D96** (2017) 014009, Erratum ibid. **D96** (2017) 039902, arXiv:1704.04082.

[39] C. S. An and H. Chen, *Observed Ω_c^0 resonances as pentaquark states*, Phys. Rev. **D96** (2017) 034012, arXiv:1705.08571.

[40] A. Ali *et al.*, *A new look at the Y tetraquarks and Ω_c baryons in the diquark model*, Eur. Phys. J. **C78** (2018) 29, arXiv:1708.04650.

[41] G. Montaña, A. Feijoo, and A. Ramos, *A meson-baryon molecular interpretation for some Ω_c excited states*, Eur. Phys. J. **A54** (2018) 64, arXiv:1709.08737.

[42] V. R. Debastiani, J. M. Dias, W. H. Liang, and E. Oset, *Molecular Ω_c states generated from coupled meson-baryon channels*, Phys. Rev. **D97** (2018) 094035, arXiv:1710.04231.

[43] E. Santopinto *et al.*, *The Ω_c-puzzle solved by means of quark model predictions*, Eur. Phys. J. C **79** (2019) 1012, arXiv:1811.01799.

[44] V. R. Debastiani, J. M. Dias, W.-H. Liang, and E. Oset, $\Omega_b^- \to (\Xi_c^+ K^-)\pi^-$ and the Ω_c states, Phys. Rev. **D98** (2018) 094022, arXiv:1803.03268.

[45] C.-K. Chua, Color-allowed bottom baryon to s-wave and p-wave charmed baryon nonleptonic decays, Phys. Rev. **D100** (2019) 034025, arXiv:1905.00153.

[46] LHCb collaboration, A. A. Alves Jr. et al., The LHCb detector at the LHC, JINST **3** (2008) S08005.

[47] LHCb collaboration, R. Aaij et al., LHCb detector performance, Int. J. Mod. Phys. **A30** (2015) 1530022, arXiv:1412.6352.

[48] T. Sjöstrand, S. Mrenna, and P. Skands, A brief introduction to PYTHIA 8.1, Comput. Phys. Commun. **178** (2008) 852, arXiv:0710.3820; T. Sjöstrand, S. Mrenna, and P. Skands, PYTHIA 6.4 physics and manual, JHEP **05** (2006) 026, arXiv:hep-ph/0603175.

[49] I. Belyaev et al., Handling of the generation of primary events in Gauss, the LHCb simulation framework, J. Phys. Conf. Ser. **331** (2011) 032047.

[50] D. J. Lange, The EvtGen particle decay simulation package, Nucl. Instrum. Meth. **A462** (2001) 152.

[51] Geant4 collaboration, J. Allison et al., Geant4 developments and applications, IEEE Trans. Nucl. Sci. **53** (2006) 270; Geant4 collaboration, S. Agostinelli et al., Geant4: A simulation toolkit, Nucl. Instrum. Meth. **A506** (2003) 250.

[52] M. Clemencic et al., The LHCb simulation application, Gauss: Design, evolution and experience, J. Phys. Conf. Ser. **331** (2011) 032023.

[53] H. Voss, A. Hoecker, J. Stelzer, and F. Tegenfeldt, TMVA - Toolkit for Multivariate Data Analysis with ROOT, PoS **ACAT** (2007) 040; A. Hoecker et al., TMVA 4 — Toolkit for Multivariate Data Analysis with ROOT. Users Guide., arXiv:physics/0703039.

[54] G. Punzi, Sensitivity of searches for new signals and its optimization, eConf **C030908** (2003) MODT002, arXiv:physics/0308063.

[55] W. D. Hulsbergen, Decay chain fitting with a Kalman filter, Nucl. Instrum. Meth. **A552** (2005) 566, arXiv:physics/0503191.

[56] Particle Data Group, P. A. Zyla et al., Review of particle physics, Prog. Theor. Exp. Phys. **2020** (2020) 083C01.

[57] G. A. Cowan, D. C. Craik, and M. D. Needham, RapidSim: an application for the fast simulation of heavy-quark hadron decays, Comput. Phys. Commun. **214** (2017) 239, arXiv:1612.07489.

[58] R. De Maesschalck, D. Jouan-Rimbaud, and D. L. Massart, The Mahalanobis distance, Chemometrics and Intelligent Laboratory Systems **50** (2000) 1.

[59] See Supplemental Material at `http://link.aps.org/supplemental/10.1103/PhysRevD.104.L091102` for tables of systematic uncertainties and additional plots.

[60] LHCb collaboration, R. Aaij *et al.*, *Precision measurement of D meson mass differences*, JHEP **06** (2013) 065, `arXiv:1304.6865`.

[61] J. M. Blatt and V. F. Weisskopf, *Theoretical nuclear physics*, Springer, New York, 1952.

[62] F. Von Hippel and C. Quigg, *Centrifugal-barrier effects in resonance partial decay widths, shapes, and production amplitudes*, Phys. Rev. **D5** (1972) 624.

[63] LHCb collaboration, R. Aaij *et al.*, *Measurements of the mass and lifetime of the Ω_b^- baryon*, Phys. Rev. **D93** (2016) 092007, `arXiv:1604.01412`.

[64] LHCb collaboration, R. Aaij *et al.*, *Measurements of the Λ_b^0, Ξ_b^-, and Ω_b^- baryon masses*, Phys. Rev. Lett. **110** (2013) 182001, `arXiv:1302.1072`.

Supplemental material for LHCb-PAPER-2021-012

The mass distributions, $m(\Xi_c^+ K^- \pi^-)$ and $m(\Omega_c^0 \pi^-)$, are shown in Fig. 5 with a logarithmic scale.
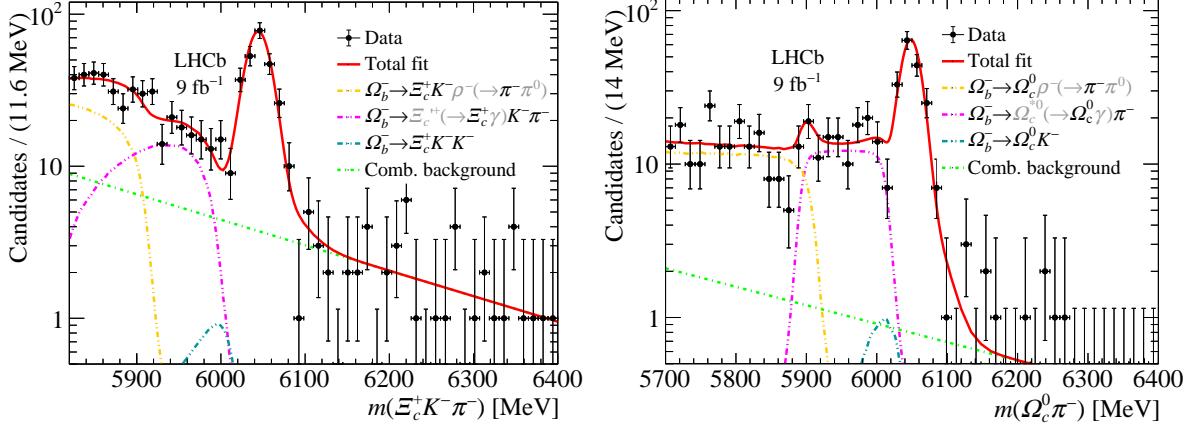
Figure 5: Distribution of the reconstructed invariant mass (left) $m(\Xi_c^+ K^- \pi^-)$ with $\Xi_c^+ \to pK^-\pi^+$ and (right) $m(\Omega_c^0 \pi^-)$ with $\Omega_c^0 \to pK^-K^-\pi^+$ using a logarithmic scale for all candidates passing the selection requirements. The black symbols show the selected signal candidates. The result of a fit is overlaid (solid red line). The missing particles in partially reconstructed decays are indicated in grey in the legends.

The $\Xi_c^+ K^- \pi^-$ mass distribution used for the investigation of the Ω_c^{**0} states is shown in Fig. 6, where a new BDT classifier is trained with the addition of the requirement $m(\Xi_c^+ K^-) < 3.3\,\text{GeV}$ in the simulation. Figure 7 shows all measurements of the Ω_b^- mass
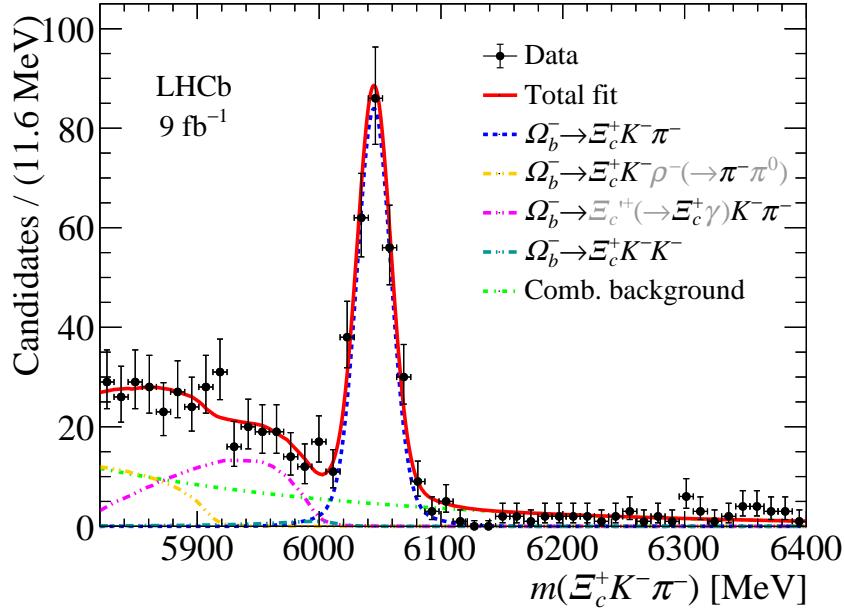
Figure 6: Distribution of the reconstructed invariant mass $m(\Xi_c^+ K^- \pi^-)$ with $\Xi_c^+ \to pK^-\pi^+$, where the simulation used to train the BDT classifier has a requirement of $m(\Xi_c^+ K^-) < 3.3\,\text{GeV}$.
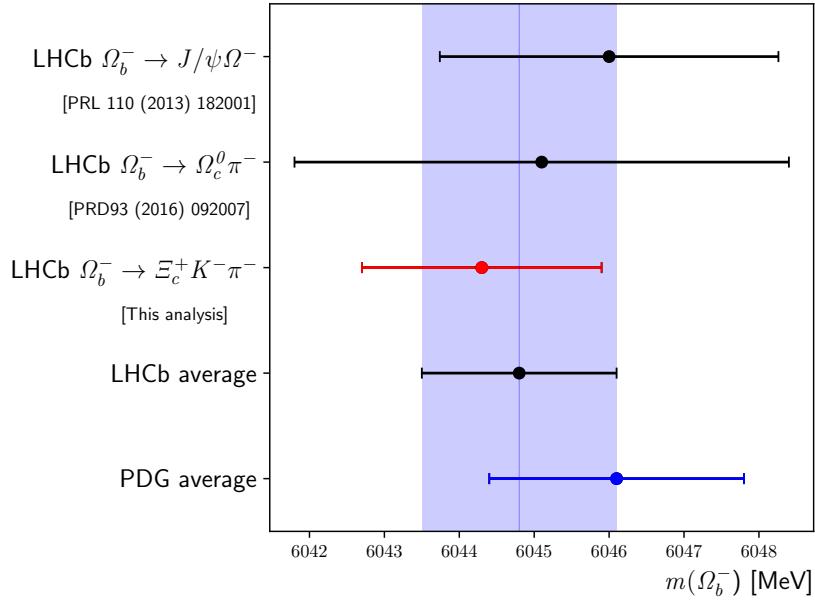
Figure 7: Measurements of the Ω_b^- mass from the LHCb experiment, the LHCb average and the PDG average, which includes the two previous LHCb measurements and one measurement from the CDF collaboration [56].

from the LHCb experiment, the LHCb average which is calculated using the Ω_b^- mass determined in this analysis and the two previous results, and the PDG average.

The efficiency map of the data reconstruction and selection in the $[\Delta M, \cos\theta]$ plane is shown in Fig. 8, where the positions of four of the Ω_c^{**0} states are demonstrated by the red lines. Figure 9 shows the value of the test statistic observables $t_{J=1/2|J=3/2}$ and $t_{J=3/2|J=5/2}$ for each Ω_c^{**0} state, where the red point indicates the value determined from data.
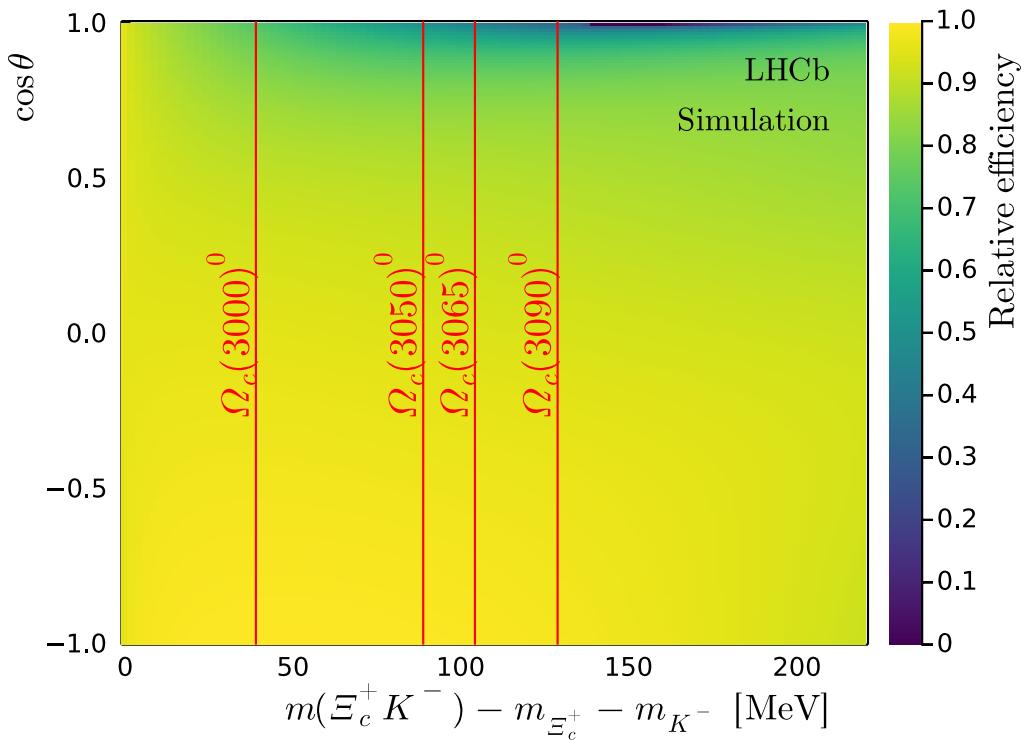
Figure 8: Efficiency map in the $[\Delta M, \cos\theta]$ plane. Positions of the four narrow Ω_c^{**0} states are shown by the red lines.
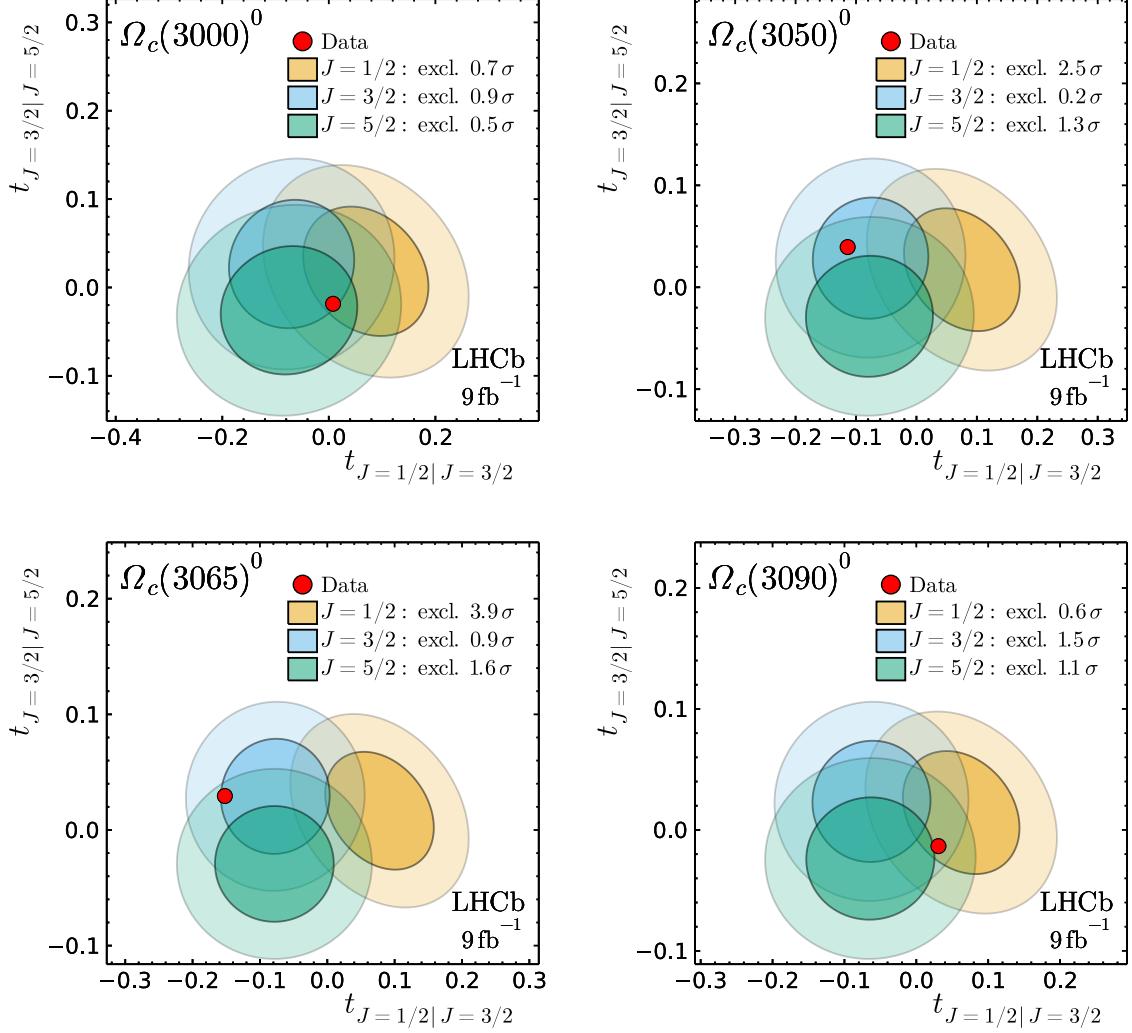
Figure 9: Values of the spin-hypothesis estimators $t_{J=1/2|J=3/2}$ and $t_{J=3/2|J=5/2}$. The red point shows the value measured in the default fit to the data. The colored ellipses give the 67 % and 95 % confidence intervals in the probability density for spin hypotheses with $J = 1/2$, $3/2$, and $5/2$ as indicated in the legend. The rejection significance of every spin-J hypothesis are shown in the legend for the default fit. The values with systematic studies included are summarised in the Table 1 of the main text.

Tables 2 and 3 summarise the systematic uncertainties considered for each observable where the largest deviation from the default model is quoted on every source.

Table 2: Systematic uncertainties in the Ω_b^- mass, relative branching fraction $\mathcal{R}$, and relative production rate $\mathcal{P}$ of the Ω_c^{**0} states.

Source	Ω_b^- $m\,[\mathrm{MeV}]$	$\mathcal{R}$	$\Omega_c(3000)^0$ $\mathcal{P}$	$\Omega_c(3050)^0$ $\mathcal{P}$	$\Omega_c(3065)^0$ $\mathcal{P}$	$\Omega_c(3090)^0$ $\mathcal{P}$
Alternative Ω_b^- fit	< 0.1	0.05	< 0.01	< 0.01	< 0.01	< 0.01
Ξ_c^+ Dalitz weights	0.5	< 0.01	0.03	0.01	< 0.01	0.02
Momentum calibration	0.9	—	—	—	—	—
PID efficiency	0.2	0.01	< 0.01	0.02	0.01	0.03
Ω_b^- kinematics	0.4	< 0.01	0.01	< 0.01	0.01	0.01
Alternative $\Xi_c^+ K^-$ fit	—	—	0.02	0.01	0.02	0.01
Efficiency map	—	< 0.01	< 0.01	< 0.01	< 0.01	< 0.01
Background in $\Xi_c^+ K^-$	—	—	< 0.01	< 0.01	< 0.01	< 0.01
Total	1.1	0.05	0.04	0.02	0.02	0.04

Table 3: Systematic uncertainties in the resonance parameters of the Ω_c^{**0} states. For the width of the $\Omega_c(3050)^0$ baryon, the systematic uncertainties are embedded in the upper limit.

Source	$\Omega_c(3000)^0$ $m\,[\mathrm{MeV}]$	$\Gamma\,[\mathrm{MeV}]$	$\Omega_c(3050)^0$ $m\,[\mathrm{MeV}]$	$\Omega_c(3065)^0$ $m\,[\mathrm{MeV}]$	$\Gamma\,[\mathrm{MeV}]$	$\Omega_c(3090)^0$ $m\,[\mathrm{MeV}]$	$\Gamma\,[\mathrm{MeV}]$
Alternative Ω_b^- fit	< 0.01	< 0.01	< 0.01	< 0.01	< 0.01	< 0.01	< 0.01
Ξ_c^+ Dalitz weights	0.02	1.1	0.10	0.14	0.2	0.32	1.2
Momentum calibration	0.01	—	0.03	0.03	—	0.04	—
PID efficiency	0.56	0.1	0.05	0.14	0.2	0.73	2.1
Ω_b^- kinematics	0.13	0.7	0.10	0.21	0.2	0.42	0.9
Alternative $\Xi_c^+ K^-$ fit	0.70	2.1	0.10	0.28	0.4	0.39	0.9
Efficiency map	< 0.01	< 0.01	< 0.01	< 0.01	< 0.01	< 0.01	< 0.01
Background in $\Xi_c^+ K^-$	0.02	0.1	< 0.01	< 0.01	0.04	< 0.01	0.2
Total	0.9	2.5	0.2	0.4	0.5	1.0	2.8

LHCb collaboration

R. Aaij[32], C. Abellán Beteta[50], T. Ackernley[60], B. Adeva[46], M. Adinolfi[54], H. Afsharnia[9],
C.A. Aidala[86], S. Aiola[25], Z. Ajaltouni[9], S. Akar[65], J. Albrecht[15], F. Alessio[48], M. Alexander[59],
A. Alfonso Albero[45], Z. Aliouche[62], G. Alkhazov[38], P. Alvarez Cartelle[55], S. Amato[2],
Y. Amhis[11], L. An[48], L. Anderlini[22], A. Andreianov[38], M. Andreotti[21], F. Archilli[17],
A. Artamonov[44], M. Artuso[68], K. Arzymatov[42], E. Aslanides[10], M. Atzeni[50], B. Audurier[12],
S. Bachmann[17], M. Bachmayer[49], J.J. Back[56], P. Baladron Rodriguez[46], V. Balagura[12],
W. Baldini[21], J. Baptista Leite[1], R.J. Barlow[62], S. Barsuk[11], W. Barter[61], M. Bartolini[24],
F. Baryshnikov[83], J.M. Basels[14], G. Bassi[29], B. Batsukh[68], A. Battig[15], A. Bay[49], M. Becker[15],
F. Bedeschi[29], I. Bediaga[1], A. Beiter[68], V. Belavin[42], S. Belin[27], V. Bellee[49], K. Belous[44],
I. Belov[40], I. Belyaev[41], G. Bencivenni[23], E. Ben-Haim[13], A. Berezhnoy[40], R. Bernet[50],
D. Berninghoff[17], H.C. Bernstein[68], C. Bertella[48], A. Bertolin[28], C. Betancourt[50], F. Betti[48],
Ia. Bezshyiko[50], S. Bhasin[54], J. Bhom[35], L. Bian[73], M.S. Bieker[15], S. Bifani[53], P. Billoir[13],
M. Birch[61], F.C.R. Bishop[55], A. Bitadze[62], A. Bizzeti[22,k], M. Bjørn[63], M.P. Blago[48], T. Blake[56],
F. Blanc[49], S. Blusk[68], D. Bobulska[59], J.A. Boelhauve[15], O. Boente Garcia[46], T. Boettcher[65],
A. Boldyrev[82], A. Bondar[43], N. Bondar[38,48], S. Borghi[62], M. Borisyak[42], M. Borsato[17],
J.T. Borsuk[35], S.A. Bouchiba[49], T.J.V. Bowcock[60], A. Boyer[48], C. Bozzi[21], M.J. Bradley[61],
S. Braun[66], A. Brea Rodriguez[46], M. Brodski[48], J. Brodzicka[35], A. Brossa Gonzalo[56],
D. Brundu[27], A. Buonaura[50], C. Burr[48], A. Bursche[72], A. Butkevich[39], J.S. Butter[32],
J. Buytaert[48], W. Byczynski[48], S. Cadeddu[27], H. Cai[73], R. Calabrese[21,f], L. Calefice[15,13],
L. Calero Diaz[23], S. Cali[23], R. Calladine[53], M. Calvi[26,j], M. Calvo Gomez[85],
P. Camargo Magalhaes[54], P. Campana[23], A.F. Campoverde Quezada[6], S. Capelli[26,j],
L. Capriotti[20,d], A. Carbone[20,d], G. Carboni[31], R. Cardinale[24], A. Cardini[27], I. Carli[4],
P. Carniti[26,j], L. Carus[14], K. Carvalho Akiba[32], A. Casais Vidal[46], G. Casse[60], M. Cattaneo[48],
G. Cavallero[48], S. Celani[49], J. Cerasoli[10], A.J. Chadwick[60], M.G. Chapman[54], M. Charles[13],
Ph. Charpentier[48], G. Chatzikonstantinidis[53], C.A. Chavez Barajas[60], M. Chefdeville[8],
C. Chen[3], S. Chen[4], A. Chernov[35], V. Chobanova[46], S. Cholak[49], M. Chrzaszcz[35],
A. Chubykin[38], V. Chulikov[38], P. Ciambrone[23], M.F. Cicala[56], X. Cid Vidal[46], G. Ciezarek[48],
P.E.L. Clarke[58], M. Clemencic[48], H.V. Cliff[55], J. Closier[48], J.L. Cobbledick[62], V. Coco[48],
J.A.B. Coelho[11], J. Cogan[10], E. Cogneras[9], L. Cojocariu[37], P. Collins[48], T. Colombo[48],
L. Congedo[19,c], A. Contu[27], N. Cooke[53], G. Coombs[59], I. Corredoira [46], G. Corti[48],
C.M. Costa Sobral[56], B. Couturier[48], D.C. Craik[64], J. Crkovská[67], M. Cruz Torres[1], R. Currie[58],
C.L. Da Silva[67], S. Dadabaev[83], E. Dall'Occo[15], J. Dalseno[46], C. D'Ambrosio[48], A. Danilina[41],
P. d'Argent[48], A. Davis[62], O. De Aguiar Francisco[62], K. De Bruyn[79], S. De Capua[62],
M. De Cian[49], J.M. De Miranda[1], L. De Paula[2], M. De Serio[19,c], D. De Simone[50],
P. De Simone[23], J.A. de Vries[80], C.T. Dean[67], D. Decamp[8], L. Del Buono[13], B. Delaney[55],
H.-P. Dembinski[15], A. Dendek[34], V. Denysenko[50], D. Derkach[82], O. Deschamps[9], F. Desse[11],
F. Dettori[27,e], B. Dey[77], A. Di Cicco[23], P. Di Nezza[23], S. Didenko[83], L. Dieste Maronas[46],
H. Dijkstra[48], V. Dobishuk[52], A.M. Donohoe[18], F. Dordei[27], A.C. dos Reis[1], L. Douglas[59],
A. Dovbnya[51], A.G. Downes[8], K. Dreimanis[60], M.W. Dudek[35], L. Dufour[48], V. Duk[78],
P. Durante[48], J.M. Durham[67], D. Dutta[62], A. Dziurda[35], A. Dzyuba[38], S. Easo[57], U. Egede[69],
V. Egorychev[41], S. Eidelman[43,v], S. Eisenhardt[58], S. Ek-In[49], L. Eklund[59,w], S. Ely[68], A. Ene[37],
E. Epple[67], S. Escher[14], J. Eschle[50], S. Esen[13], T. Evans[48], A. Falabella[20], J. Fan[3], Y. Fan[6],
B. Fang[73], S. Farry[60], D. Fazzini[26,j], M. Féo[48], A. Fernandez Prieto[46],
J.M. Fernandez-tenllado Arribas[45], A.D. Fernez[66], F. Ferrari[20,d], L. Ferreira Lopes[49],
F. Ferreira Rodrigues[2], S. Ferreres Sole[32], M. Ferrillo[50], M. Ferro-Luzzi[48], S. Filippov[39],
R.A. Fini[19], M. Fiorini[21,f], M. Firlej[34], K.M. Fischer[63], D.S. Fitzgerald[86], C. Fitzpatrick[62],
T. Fiutowski[34], A. Fkiaras[48], F. Fleuret[12], M. Fontana[13], F. Fontanelli[24,h], R. Forty[48],
V. Franco Lima[60], M. Franco Sevilla[66], M. Frank[48], E. Franzoso[21], G. Frau[17], C. Frei[48],

D.A. Friday[59], J. Fu[25], Q. Fuehring[15], W. Funk[48], E. Gabriel[32], T. Gaintseva[42],
A. Gallas Torreira[46], D. Galli[20,d], S. Gambetta[58,48], Y. Gan[3], M. Gandelman[2], P. Gandini[25],
Y. Gao[5], M. Garau[27], L.M. Garcia Martin[56], P. Garcia Moreno[45], J. García Pardiñas[26,j],
B. Garcia Plana[46], F.A. Garcia Rosales[12], L. Garrido[45], C. Gaspar[48], R.E. Geertsema[32],
D. Gerick[17], L.L. Gerken[15], E. Gersabeck[62], M. Gersabeck[62], T. Gershon[56], D. Gerstel[10],
Ph. Ghez[8], V. Gibson[55], H.K. Giemza[36], M. Giovannetti[23,p], A. Gioventù[46],
P. Gironella Gironell[45], L. Giubega[37], C. Giugliano[21,f,48], K. Gizdov[58], E.L. Gkougkousis[48],
V.V. Gligorov[13], C. Göbel[70], E. Golobardes[85], D. Golubkov[41], A. Golutvin[61,83], A. Gomes[1,a],
S. Gomez Fernandez[45], F. Goncalves Abrantes[63], M. Goncerz[35], G. Gong[3], P. Gorbounov[41],
I.V. Gorelov[40], C. Gotti[26], E. Govorkova[48], J.P. Grabowski[17], T. Grammatico[13],
L.A. Granado Cardoso[48], E. Graugés[45], E. Graverini[49], G. Graziani[22], A. Grecu[37],
L.M. Greeven[32], P. Griffith[21,f], L. Grillo[62], S. Gromov[83], B.R. Gruberg Cazon[63], C. Gu[3],
M. Guarise[21], P. A. Günther[17], E. Gushchin[39], A. Guth[14], Y. Guz[44], T. Gys[48],
T. Hadavizadeh[69], G. Haefeli[49], C. Haen[48], J. Haimberger[48], T. Halewood-leagas[60],
P.M. Hamilton[66], J.P. Hammerich[60], Q. Han[7], X. Han[17], T.H. Hancock[63],
S. Hansmann-Menzemer[17], N. Harnew[63], T. Harrison[60], C. Hasse[48], M. Hatch[48], J. He[6,b],
M. Hecker[61], K. Heijhoff[32], K. Heinicke[15], A.M. Hennequin[48], K. Hennessy[60], L. Henry[48],
J. Heuel[14], A. Hicheur[2], D. Hill[49], M. Hilton[62], S.E. Hollitt[15], J. Hu[17], J. Hu[72], W. Hu[7],
X. Hu[3], W. Huang[6], X. Huang[73], W. Hulsbergen[32], R.J. Hunter[56], M. Hushchyn[82],
D. Hutchcroft[60], D. Hynds[32], P. Ibis[15], M. Idzik[34], D. Ilin[38], P. Ilten[65], A. Inglessi[38],
A. Ishteev[83], K. Ivshin[38], R. Jacobsson[48], S. Jakobsen[48], E. Jans[32], B.K. Jashal[47],
A. Jawahery[66], V. Jevtic[15], M. Jezabek[35], F. Jiang[3], M. John[63], D. Johnson[48], C.R. Jones[55],
T.P. Jones[56], B. Jost[48], N. Jurik[48], S. Kandybei[51], Y. Kang[3], M. Karacson[48], M. Karpov[82],
F. Keizer[48], M. Kenzie[56], T. Ketel[33], B. Khanji[15], A. Kharisova[84], S. Kholodenko[44], T. Kirn[14],
V.S. Kirsebom[49], O. Kitouni[64], S. Klaver[32], K. Klimaszewski[36], S. Koliiev[52], A. Kondybayeva[83],
A. Konoplyannikov[41], P. Kopciewicz[34], R. Kopecna[17], P. Koppenburg[32], M. Korolev[40],
I. Kostiuk[32,52], O. Kot[52], S. Kotriakhova[21,38], P. Kravchenko[38], L. Kravchuk[39],
R.D. Krawczyk[48], M. Kreps[56], F. Kress[61], S. Kretzschmar[14], P. Krokovny[43,v], W. Krupa[34],
W. Krzemien[36], W. Kucewicz[35,t], M. Kucharczyk[35], V. Kudryavtsev[43,v], H.S. Kuindersma[32,33],
G.J. Kunde[67], T. Kvaratskheliya[41], D. Lacarrere[48], G. Lafferty[62], A. Lai[27], A. Lampis[27],
D. Lancierini[50], J.J. Lane[62], R. Lane[54], G. Lanfranchi[23], C. Langenbruch[14], J. Langer[15],
O. Lantwin[50], T. Latham[56], F. Lazzari[29,q], R. Le Gac[10], S.H. Lee[86], R. Lefèvre[9], A. Leflat[40],
S. Legotin[83], O. Leroy[10], T. Lesiak[35], B. Leverington[17], H. Li[72], L. Li[63], P. Li[17], S. Li[7], Y. Li[4],
Y. Li[4], Z. Li[68], X. Liang[68], T. Lin[61], R. Lindner[48], V. Lisovskyi[15], R. Litvinov[27], G. Liu[72],
H. Liu[6], S. Liu[4], A. Loi[27], J. Lomba Castro[46], I. Longstaff[59], J.H. Lopes[2], G.H. Lovell[55], Y. Lu[4],
D. Lucchesi[28,l], S. Luchuk[39], M. Lucio Martinez[32], V. Lukashenko[32], Y. Luo[3], A. Lupato[62],
E. Luppi[21,f], O. Lupton[56], A. Lusiani[29,m], X. Lyu[6], L. Ma[4], R. Ma[6], S. Maccolini[20,d],
F. Machefert[11], F. Maciuc[37], V. Macko[49], P. Mackowiak[15], S. Maddrell-Mander[54],
O. Madejczyk[34], L.R. Madhan Mohan[54], O. Maev[38], A. Maevskiy[82], D. Maisuzenko[38],
M.W. Majewski[34], J.J. Malczewski[35], S. Malde[63], B. Malecki[48], A. Malinin[81], T. Maltsev[43,v],
H. Malygina[17], G. Manca[27,e], G. Mancinelli[10], D. Manuzzi[20,d], D. Marangotto[25,i], J. Maratas[9,s],
J.F. Marchand[8], U. Marconi[20], S. Mariani[22,g], C. Marin Benito[48], M. Marinangeli[49], J. Marks[17],
A.M. Marshall[54], P.J. Marshall[60], G. Martellotti[30], L. Martinazzoli[48,j], M. Martinelli[26,j],
D. Martinez Santos[46], F. Martinez Vidal[47], A. Massafferri[1], M. Materok[14], R. Matev[48],
A. Mathad[50], Z. Mathe[48], V. Matiunin[41], C. Matteuzzi[26], K.R. Mattioli[86], A. Mauri[32],
E. Maurice[12], J. Mauricio[45], M. Mazurek[48], M. McCann[61], L. Mcconnell[18], T.H. Mcgrath[62],
A. McNab[62], R. McNulty[18], J.V. Mead[60], B. Meadows[65], G. Meier[15], N. Meinert[76],
D. Melnychuk[36], S. Meloni[26,j], M. Merk[32,80], A. Merli[25], L. Meyer Garcia[2], M. Mikhasenko[48],
D.A. Milanes[74], E. Millard[56], M. Milovanovic[48], M.-N. Minard[8], A. Minotti[21], L. Minzoni[21,f],
S.E. Mitchell[58], B. Mitreska[62], D.S. Mitzel[48], A. Mödden [15], R.A. Mohammed[63], R.D. Moise[61],

T. Mombächer[46], I.A. Monroy[74], S. Monteil[9], M. Morandin[28], G. Morello[23], M.J. Morello[29,m],
J. Moron[34], A.B. Morris[75], A.G. Morris[56], R. Mountain[68], H. Mu[3], F. Muheim[58,48],
M. Mulder[48], D. Müller[48], K. Müller[50], C.H. Murphy[63], D. Murray[62], P. Muzzetto[27,48],
P. Naik[54], T. Nakada[49], R. Nandakumar[57], T. Nanut[49], I. Nasteva[2], M. Needham[58], I. Neri[21],
N. Neri[25,i], S. Neubert[75], N. Neufeld[48], R. Newcombe[61], T.D. Nguyen[49], C. Nguyen-Mau[49,x],
E.M. Niel[11], S. Nieswand[14], N. Nikitin[40], N.S. Nolte[64], C. Normand[8], C. Nunez[86],
A. Oblakowska-Mucha[34], V. Obraztsov[44], D.P. O'Hanlon[54], R. Oldeman[27,e], M.E. Olivares[68],
C.J.G. Onderwater[79], R.H. O'neil[58], A. Ossowska[35], J.M. Otalora Goicochea[2],
T. Ovsiannikova[41], P. Owen[50], A. Oyanguren[47], B. Pagare[56], P.R. Pais[48], T. Pajero[63],
A. Palano[19], M. Palutan[23], Y. Pan[62], G. Panshin[84], A. Papanestis[57], M. Pappagallo[19,c],
L.L. Pappalardo[21,f], C. Pappenheimer[65], W. Parker[66], C. Parkes[62], C.J. Parkinson[46],
B. Passalacqua[21], G. Passaleva[22], A. Pastore[19], M. Patel[61], C. Patrignani[20,d], C.J. Pawley[80],
A. Pearce[48], A. Pellegrino[32], M. Pepe Altarelli[48], S. Perazzini[20], D. Pereima[41], P. Perret[9],
I. Petrenko[52], M. Petric[59,48], K. Petridis[54], A. Petrolini[24,h], A. Petrov[81], S. Petrucci[58],
M. Petruzzo[25], T.T.H. Pham[68], A. Philippov[42], L. Pica[29,m], M. Piccini[78], B. Pietrzyk[8],
G. Pietrzyk[49], M. Pili[63], D. Pinci[30], F. Pisani[48], Resmi P.K[10], V. Placinta[37], J. Plews[53],
M. Plo Casasus[46], F. Polci[13], M. Poli Lener[23], M. Poliakova[68], A. Poluektov[10], N. Polukhina[83,u],
I. Polyakov[68], E. Polycarpo[2], G.J. Pomery[54], S. Ponce[48], D. Popov[6,48], S. Popov[42],
S. Poslavskii[44], K. Prasanth[35], L. Promberger[48], C. Prouve[46], V. Pugatch[52], H. Pullen[63],
G. Punzi[29,n], H. Qi[3], W. Qian[6], J. Qin[6], N. Qin[3], R. Quagliani[13], B. Quintana[8], N.V. Raab[18],
R.I. Rabadan Trejo[10], B. Rachwal[34], J.H. Rademacker[54], M. Rama[29], M. Ramos Pernas[56],
M.S. Rangel[2], F. Ratnikov[42,82], G. Raven[33], M. Reboud[8], F. Redi[49], F. Reiss[62],
C. Remon Alepuz[47], Z. Ren[3], V. Renaudin[63], R. Ribatti[29], S. Ricciardi[57], K. Rinnert[60],
P. Robbe[11], G. Robertson[58], A.B. Rodrigues[49], E. Rodrigues[60], J.A. Rodriguez Lopez[74],
E.R.R. Rodriguez Rodriguez[46], A. Rollings[63], P. Roloff[48], V. Romanovskiy[44],
M. Romero Lamas[46], A. Romero Vidal[46], J.D. Roth[86], M. Rotondo[23], M.S. Rudolph[68],
T. Ruf[48], J. Ruiz Vidal[47], A. Ryzhikov[82], J. Ryzka[34], J.J. Saborido Silva[46], N. Sagidova[38],
N. Sahoo[56], B. Saitta[27,e], M. Salomoni[48], D. Sanchez Gonzalo[45], C. Sanchez Gras[32],
R. Santacesaria[30], C. Santamarina Rios[46], M. Santimaria[23], E. Santovetti[31,p], D. Saranin[83],
G. Sarpis[59], M. Sarpis[75], A. Sarti[30], C. Satriano[30,o], A. Satta[31], M. Saur[15], D. Savrina[41,40],
H. Sazak[9], L.G. Scantlebury Smead[63], A. Scarabotto[13], S. Schael[14], M. Schiller[59],
H. Schindler[48], M. Schmelling[16], B. Schmidt[48], O. Schneider[49], A. Schopper[48], M. Schubiger[32],
S. Schulte[49], M.H. Schune[11], R. Schwemmer[48], B. Sciascia[23], S. Sellam[46], A. Semennikov[41],
M. Senghi Soares[33], A. Sergi[24], N. Serra[50], L. Sestini[28], A. Seuthe[15], P. Seyfert[48], Y. Shang[5],
D.M. Shangase[86], M. Shapkin[44], I. Shchemerov[83], L. Shchutska[49], T. Shears[60],
L. Shekhtman[43,v], Z. Shen[5], V. Shevchenko[81], E.B. Shields[26,j], E. Shmanin[83], J.D. Shupperd[68],
B.G. Siddi[21], R. Silva Coutinho[50], G. Simi[28], S. Simone[19,c], N. Skidmore[62], T. Skwarnicki[68],
M.W. Slater[53], I. Slazyk[21,f], J.C. Smallwood[63], J.G. Smeaton[55], A. Smetkina[41], E. Smith[50],
M. Smith[61], A. Snoch[32], M. Soares[20], L. Soares Lavra[9], M.D. Sokoloff[65], F.J.P. Soler[59],
A. Solovev[38], I. Solovyev[38], F.L. Souza De Almeida[2], B. Souza De Paula[2], B. Spaan[15],
E. Spadaro Norella[25,i], P. Spradlin[59], F. Stagni[48], M. Stahl[65], S. Stahl[48], P. Stefko[49],
O. Steinkamp[50,83], O. Stenyakin[44], H. Stevens[15], S. Stone[68], M.E. Stramaglia[49], M. Straticiuc[37],
D. Strekalina[83], F. Suljik[63], J. Sun[27], L. Sun[73], Y. Sun[66], P. Svihra[62], P.N. Swallow[53],
K. Swientek[34], A. Szabelski[36], T. Szumlak[34], M. Szymanski[48], S. Taneja[62], A.R. Tanner[54],
A. Terentev[83], F. Teubert[48], E. Thomas[48], K.A. Thomson[60], V. Tisserand[9], S. T'Jampens[8],
M. Tobin[4], L. Tomassetti[21,f], D. Torres Machado[1], D.Y. Tou[13], M.T. Tran[49], E. Trifonova[83],
C. Trippl[49], G. Tuci[29,n], A. Tully[49], N. Tuning[32,48], A. Ukleja[36], D.J. Unverzagt[17], E. Ursov[83],
A. Usachov[32], A. Ustyuzhanin[42,82], U. Uwer[17], A. Vagner[84], V. Vagnoni[20], A. Valassi[48],
G. Valenti[20], N. Valls Canudas[85], M. van Beuzekom[32], M. Van Dijk[49], E. van Herwijnen[83],
C.B. Van Hulse[18], M. van Veghel[79], R. Vazquez Gomez[46], P. Vazquez Regueiro[46],

23

C. Vázquez Sierra[48], S. Vecchi[21], J.J. Velthuis[54], M. Veltri[22,r], A. Venkateswaran[68],
M. Veronesi[32], M. Vesterinen[56], D. Vieira[65], M. Vieites Diaz[49], H. Viemann[76],
X. Vilasis-Cardona[85], E. Vilella Figueras[60], A. Villa[20], P. Vincent[13], D. Vom Bruch[10],
A. Vorobyev[38], V. Vorobyev[43,v], N. Voropaev[38], K. Vos[80], R. Waldi[17], J. Walsh[29], C. Wang[17],
J. Wang[5], J. Wang[4], J. Wang[3], J. Wang[73], M. Wang[3], R. Wang[54], Y. Wang[7], Z. Wang[50],
Z. Wang[3], H.M. Wark[60], N.K. Watson[53], S.G. Weber[13], D. Websdale[61], C. Weisser[64],
B.D.C. Westhenry[54], D.J. White[62], M. Whitehead[54], D. Wiedner[15], G. Wilkinson[63],
M. Wilkinson[68], I. Williams[55], M. Williams[64], M.R.J. Williams[58], F.F. Wilson[57], W. Wislicki[36],
M. Witek[35], L. Witola[17], G. Wormser[11], S.A. Wotton[55], H. Wu[68], K. Wyllie[48], Z. Xiang[6],
D. Xiao[7], Y. Xie[7], A. Xu[5], J. Xu[6], L. Xu[3], M. Xu[7], Q. Xu[6], Z. Xu[5], Z. Xu[6], D. Yang[3],
S. Yang[6], Y. Yang[6], Z. Yang[3], Z. Yang[66], Y. Yao[68], L.E. Yeomans[60], H. Yin[7], J. Yu[71],
X. Yuan[68], O. Yushchenko[44], E. Zaffaroni[49], M. Zavertyaev[16,u], M. Zdybal[35], O. Zenaiev[48],
M. Zeng[3], D. Zhang[7], L. Zhang[3], S. Zhang[5], Y. Zhang[5], Y. Zhang[63], A. Zharkova[83],
A. Zhelezov[17], Y. Zheng[6], X. Zhou[6], Y. Zhou[6], X. Zhu[3], Z. Zhu[6], V. Zhukov[14,40],
J.B. Zonneveld[58], Q. Zou[4], S. Zucchelli[20,d], D. Zuliani[28], G. Zunica[62].

[1]Centro Brasileiro de Pesquisas Físicas (CBPF), Rio de Janeiro, Brazil
[2]Universidade Federal do Rio de Janeiro (UFRJ), Rio de Janeiro, Brazil
[3]Center for High Energy Physics, Tsinghua University, Beijing, China
[4]Institute Of High Energy Physics (IHEP), Beijing, China
[5]School of Physics State Key Laboratory of Nuclear Physics and Technology, Peking University, Beijing,
China
[6]University of Chinese Academy of Sciences, Beijing, China
[7]Institute of Particle Physics, Central China Normal University, Wuhan, Hubei, China
[8]Univ. Savoie Mont Blanc, CNRS, IN2P3-LAPP, Annecy, France
[9]Université Clermont Auvergne, CNRS/IN2P3, LPC, Clermont-Ferrand, France
[10]Aix Marseille Univ, CNRS/IN2P3, CPPM, Marseille, France
[11]Université Paris-Saclay, CNRS/IN2P3, IJCLab, Orsay, France
[12]Laboratoire Leprince-Ringuet, CNRS/IN2P3, Ecole Polytechnique, Institut Polytechnique de Paris,
Palaiseau, France
[13]LPNHE, Sorbonne Université, Paris Diderot Sorbonne Paris Cité, CNRS/IN2P3, Paris, France
[14]I. Physikalisches Institut, RWTH Aachen University, Aachen, Germany
[15]Fakultät Physik, Technische Universität Dortmund, Dortmund, Germany
[16]Max-Planck-Institut für Kernphysik (MPIK), Heidelberg, Germany
[17]Physikalisches Institut, Ruprecht-Karls-Universität Heidelberg, Heidelberg, Germany
[18]School of Physics, University College Dublin, Dublin, Ireland
[19]INFN Sezione di Bari, Bari, Italy
[20]INFN Sezione di Bologna, Bologna, Italy
[21]INFN Sezione di Ferrara, Ferrara, Italy
[22]INFN Sezione di Firenze, Firenze, Italy
[23]INFN Laboratori Nazionali di Frascati, Frascati, Italy
[24]INFN Sezione di Genova, Genova, Italy
[25]INFN Sezione di Milano, Milano, Italy
[26]INFN Sezione di Milano-Bicocca, Milano, Italy
[27]INFN Sezione di Cagliari, Monserrato, Italy
[28]Universita degli Studi di Padova, Universita e INFN, Padova, Padova, Italy
[29]INFN Sezione di Pisa, Pisa, Italy
[30]INFN Sezione di Roma La Sapienza, Roma, Italy
[31]INFN Sezione di Roma Tor Vergata, Roma, Italy
[32]Nikhef National Institute for Subatomic Physics, Amsterdam, Netherlands
[33]Nikhef National Institute for Subatomic Physics and VU University Amsterdam, Amsterdam,
Netherlands
[34]AGH - University of Science and Technology, Faculty of Physics and Applied Computer Science,
Kraków, Poland
[35]Henryk Niewodniczanski Institute of Nuclear Physics Polish Academy of Sciences, Kraków, Poland

[36] *National Center for Nuclear Research (NCBJ), Warsaw, Poland*
[37] *Horia Hulubei National Institute of Physics and Nuclear Engineering, Bucharest-Magurele, Romania*
[38] *Petersburg Nuclear Physics Institute NRC Kurchatov Institute (PNPI NRC KI), Gatchina, Russia*
[39] *Institute for Nuclear Research of the Russian Academy of Sciences (INR RAS), Moscow, Russia*
[40] *Institute of Nuclear Physics, Moscow State University (SINP MSU), Moscow, Russia*
[41] *Institute of Theoretical and Experimental Physics NRC Kurchatov Institute (ITEP NRC KI), Moscow, Russia*
[42] *Yandex School of Data Analysis, Moscow, Russia*
[43] *Budker Institute of Nuclear Physics (SB RAS), Novosibirsk, Russia*
[44] *Institute for High Energy Physics NRC Kurchatov Institute (IHEP NRC KI), Protvino, Russia, Protvino, Russia*
[45] *ICCUB, Universitat de Barcelona, Barcelona, Spain*
[46] *Instituto Galego de Física de Altas Enerxías (IGFAE), Universidade de Santiago de Compostela, Santiago de Compostela, Spain*
[47] *Instituto de Fisica Corpuscular, Centro Mixto Universidad de Valencia - CSIC, Valencia, Spain*
[48] *European Organization for Nuclear Research (CERN), Geneva, Switzerland*
[49] *Institute of Physics, Ecole Polytechnique Fédérale de Lausanne (EPFL), Lausanne, Switzerland*
[50] *Physik-Institut, Universität Zürich, Zürich, Switzerland*
[51] *NSC Kharkiv Institute of Physics and Technology (NSC KIPT), Kharkiv, Ukraine*
[52] *Institute for Nuclear Research of the National Academy of Sciences (KINR), Kyiv, Ukraine*
[53] *University of Birmingham, Birmingham, United Kingdom*
[54] *H.H. Wills Physics Laboratory, University of Bristol, Bristol, United Kingdom*
[55] *Cavendish Laboratory, University of Cambridge, Cambridge, United Kingdom*
[56] *Department of Physics, University of Warwick, Coventry, United Kingdom*
[57] *STFC Rutherford Appleton Laboratory, Didcot, United Kingdom*
[58] *School of Physics and Astronomy, University of Edinburgh, Edinburgh, United Kingdom*
[59] *School of Physics and Astronomy, University of Glasgow, Glasgow, United Kingdom*
[60] *Oliver Lodge Laboratory, University of Liverpool, Liverpool, United Kingdom*
[61] *Imperial College London, London, United Kingdom*
[62] *Department of Physics and Astronomy, University of Manchester, Manchester, United Kingdom*
[63] *Department of Physics, University of Oxford, Oxford, United Kingdom*
[64] *Massachusetts Institute of Technology, Cambridge, MA, United States*
[65] *University of Cincinnati, Cincinnati, OH, United States*
[66] *University of Maryland, College Park, MD, United States*
[67] *Los Alamos National Laboratory (LANL), Los Alamos, United States*
[68] *Syracuse University, Syracuse, NY, United States*
[69] *School of Physics and Astronomy, Monash University, Melbourne, Australia, associated to [56]*
[70] *Pontifícia Universidade Católica do Rio de Janeiro (PUC-Rio), Rio de Janeiro, Brazil, associated to [2]*
[71] *Physics and Micro Electronic College, Hunan University, Changsha City, China, associated to [7]*
[72] *Guangdong Provincial Key Laboratory of Nuclear Science, Guangdong-Hong Kong Joint Laboratory of Quantum Matter, Institute of Quantum Matter, South China Normal University, Guangzhou, China, associated to [3]*
[73] *School of Physics and Technology, Wuhan University, Wuhan, China, associated to [3]*
[74] *Departamento de Fisica , Universidad Nacional de Colombia, Bogota, Colombia, associated to [13]*
[75] *Universität Bonn - Helmholtz-Institut für Strahlen und Kernphysik, Bonn, Germany, associated to [17]*
[76] *Institut für Physik, Universität Rostock, Rostock, Germany, associated to [17]*
[77] *Eotvos Lorand University, Budapest, Hungary, associated to [48]*
[78] *INFN Sezione di Perugia, Perugia, Italy, associated to [21]*
[79] *Van Swinderen Institute, University of Groningen, Groningen, Netherlands, associated to [32]*
[80] *Universiteit Maastricht, Maastricht, Netherlands, associated to [32]*
[81] *National Research Centre Kurchatov Institute, Moscow, Russia, associated to [41]*
[82] *National Research University Higher School of Economics, Moscow, Russia, associated to [42]*
[83] *National University of Science and Technology "MISIS", Moscow, Russia, associated to [41]*
[84] *National Research Tomsk Polytechnic University, Tomsk, Russia, associated to [41]*
[85] *DS4DS, La Salle, Universitat Ramon Llull, Barcelona, Spain, associated to [45]*
[86] *University of Michigan, Ann Arbor, United States, associated to [68]*

25

[a] *Universidade Federal do Triângulo Mineiro (UFTM), Uberaba-MG, Brazil*
[b] *Hangzhou Institute for Advanced Study, UCAS, Hangzhou, China*
[c] *Università di Bari, Bari, Italy*
[d] *Università di Bologna, Bologna, Italy*
[e] *Università di Cagliari, Cagliari, Italy*
[f] *Università di Ferrara, Ferrara, Italy*
[g] *Università di Firenze, Firenze, Italy*
[h] *Università di Genova, Genova, Italy*
[i] *Università degli Studi di Milano, Milano, Italy*
[j] *Università di Milano Bicocca, Milano, Italy*
[k] *Università di Modena e Reggio Emilia, Modena, Italy*
[l] *Università di Padova, Padova, Italy*
[m] *Scuola Normale Superiore, Pisa, Italy*
[n] *Università di Pisa, Pisa, Italy*
[o] *Università della Basilicata, Potenza, Italy*
[p] *Università di Roma Tor Vergata, Roma, Italy*
[q] *Università di Siena, Siena, Italy*
[r] *Università di Urbino, Urbino, Italy*
[s] *MSU - Iligan Institute of Technology (MSU-IIT), Iligan, Philippines*
[t] *AGH - University of Science and Technology, Faculty of Computer Science, Electronics and Telecommunications, Kraków, Poland*
[u] *P.N. Lebedev Physical Institute, Russian Academy of Science (LPI RAS), Moscow, Russia*
[v] *Novosibirsk State University, Novosibirsk, Russia*
[w] *Department of Physics and Astronomy, Uppsala University, Uppsala, Sweden*
[x] *Hanoi University of Science, Hanoi, Vietnam*